First-principles study of crystal-face specificity in surface properties of Fe-rich Fe-Cr alloys

Xiaojie Li,[1,2,*] Stephan Schönecker,[2,†] Xiaoqing Li,[2] Shengzhi Hao,[1] Jijun Zhao,[1,‡] Börje Johansson,[2,3] and Levente Vitos[2,3,4]

[1]*Key Laboratory of Materials Modification by Laser, Electron, and Ion Beams (Dalian University of Technology), Ministry of Education, Dalian 116024, China*

[2]*Applied Materials Physics, Department of Materials Science and Engineering, KTH-Royal Institute of Technology, Stockholm SE-10044, Sweden*

[3]*Department of Physics and Astronomy, Division of Materials Theory, Uppsala University, Box 516, SE-75120, Uppsala, Sweden*

[4]*Research Institute for Solid State Physics and Optics, Wigner Research Center for Physics, Budapest H-1525, P.O. Box 49, Hungary*

(Received 27 November 2018; published 1 March 2019)

A density-functional theory investigation of the (100) and (110) surfaces of the body-centered cubic (bcc) $Fe_{1-x_b}Cr_{x_b}$ binary alloys, $x_b \leqslant 15$ at.%, is reported. The energies and segregation energies of these surfaces were calculated for chemically homogeneous concentration profiles and for Cr surface contents deviating from the nominal one of the bulk. The implications of these results for the surface alloy phase diagram are discussed. The surface chemistry of Fe-Cr(100) is characterized by a transition from Cr depletion to Cr enrichment in a critical bulk Cr composition window of $6 < x_b < 9$ at.%. In contrast, such threshold behavior of the surface Cr content is absent for Fe-Cr(110) and a nearly homogeneous Cr concentration profile is energetically favorable. The strongly suppressed surface-layer relaxation at both surfaces is shown to be of magnetic origin. The compressive, magnetic contribution to the surface relaxation stress is found to correlate well with the surface magnetic moment squared at both surface terminations. The stability of the Cr surface magnetic moments against bulk Cr content is clarified based on the surface electronic structure.

DOI: 10.1103/PhysRevMaterials.3.034401

I. INTRODUCTION

The bcc Fe-Cr binary system is the base of various ferritic stainless steels with numerous, technologically appealing properties, but also fundamentally interesting for its composition and structure dependent magnetic properties and observed spin-glass behavior [1]. Fe-Cr possesses spinodal decomposition in an asymmetric miscibility gap, which is skewed towards Fe-rich alloys allowing a finite Cr solubility even at low temperature. Chromium alloying imparts corrosion resistance in bcc Fe at ambient conditions through formation of a Cr-oxide surface film effectively blocking further corrosion into the bulk [2–4]. It has long been known that the corrosion rate of ferritic steel drastically reduces when the bulk Cr content exceeds ≈9–12 at.% level [5]. Understanding the necessary Cr segregation towards the surface and the formation of the protective Cr oxide scale is thus of fundamental scientific interest as well as indispensable for designing next-generation multifunctional steels, for instance, for reactor purposes [6].

The problem considered here addresses the question whether the stainlessness effect in Fe-Cr (Cr segregation) is universal in the sense that Cr would segregate to all free surfaces at above the critical composition, as opposed to a *surface-facet specific* segregation behavior (with possibly specific critical compositions). This issue arises from limited, partially conflicting theoretical and experimental data and has obviously important consequences for the understanding of oxidation resistance of ferritic materials. Most experimental and theoretical scientific attention on the surface-facet specific segregation of Cr and oxidation behavior in Fe-rich Fe-Cr was directed to the open (100) surface [2,7–16], arguably due to the belief that it is the most important cleavage plane in bcc Fe [17]. The surface composition of $Fe_{0.84}Cr_{0.16}$ observed with Auger electron spectroscopy (AES) [2,7] indicated Cr enrichment for the (100) surface when subjected to different annealing procedures with and without oxygen atmosphere. On the other hand, a scanning tunneling microscopy study [10] for layer-by-layer growth of Cr on Fe(100) determined that out of one Cr monolayer or less deposited at 300 °C only 10%–25% remained on the surface. A similar tendency for Cr migration into the subsurface layers was found for submonolayer Cr films grown on the (100) face of Fe whiskers [11], where approximately half of the Cr deposited at 296 °C was detected below the surface. Previous first-principles density-functional theory (DFT) calculations on single atom Cr segregation on Fe(100) using large simulation cells (low effective Cr concentration) essentially confirmed the picture that Cr does not energetically or entropically surface segregate in pure Fe [12–16]. Nevertheless, the surface position was energetically favorable in simulations with high effective Cr concentration [14,15].

These apparently conflicting results on the Cr migration at Fe(100) and Fe-rich, Fe-Cr(100) surfaces are resolved in a compositional threshold scenario [18–21]. Accordingly, the surface chemistry of Fe-Cr significantly changes in a narrow bulk Cr composition window below (above) which

*xiaojie2@kth.se
†stesch@kth.se
‡zhaojj@dlut.edu.cn

Cr-depleted (Cr-enriched) Fe-Cr(100) surfaces are energetically favorable. Recent DFT calculations for concentrated solid solutions using the coherent-potential approximation (CPA) determined this critical composition range to ≈8–11 at.% bulk Cr (at 0 K). It is believed that this behavior is primarily due to magnetic effects [20–22] and originates from frustration of Cr spins on the bcc lattice, which can not simultaneously be aligned antiparallel to the Fe spins and themselves. Ackland [20] showed that a lattice-based ferromagnetic-antiferromagnetic Ising model qualitatively describes the phase diagram of the Fe-Cr system, wherein the Cr bulk solubility is limited by Cr-Cr spin frustration. The onset of the preferential Cr surface precipitation on (100) oriented surfaces then coincides with the bulk solubility limit and Cr would surface segregate due to its lower cohesive energy [21]. However, this Monte Carlo study did not consider any surface physics besides the coordination number (i.e., surface-facet dependent and depth-sensitive interaction parameters) and thus can only give a limited answer on the crystal-face specificity in Cr surface segregation and the nature of the Fe-Cr surface alloy. On the other hand, it is unclear whether the DFT results and mechanisms proposed in Refs. [18,19] are transferable to other surface facets. The main point is that differences in surface electronic structure and surface magnetism may be expected to lead to different Cr solution energies and solubility, and, hence, segregation behavior.

In fact, there are few, although partially conflicting indications that the preferential segregation of Cr does not occur on other surface facets. The AES studies of Leygraf *et al.* [2,7] for $Fe_{0.84}Cr_{0.16}$ indicated Cr enrichment for the (110) surface after various annealing procedures, similar to their findings for the (100) face. Subsequent investigations [8,9] with different surface sensitive techniques for $Fe_{0.72}Cr_{0.28}$(110) confirmed a similar Cr enrichment effect after annealing. Using the CPA and a Green's-function technique for semi-infinite surfaces implemented in the tight-binding linear-muffin-tin orbitals method, Ruban *et al.* [13] determined a large positive (0.1 eV) surface segregation energy for Cr in bcc Fe(110), meaning that Cr would strongly favor desegregation from the surface, similarly to the behavior at the (100) surface. Nevertheless, Kiejna and Wachowicz [15] recently obtained a quite different result using a plane-wave basis approach: a single Cr impurity in a (110) oriented Fe slab was found to possess a negative, nearly vanishing segregation energy.

Here, we focus on the two energetically most stable surface facets of bcc Fe, (110) and (100), and investigate the compositional effect of Cr on the surface energy and surface segregation energy of Fe-rich Fe-Cr alloy with nominal bulk concentration up to 15 at.%. We provide evidence that the compositional threshold behavior of Cr does not occur at the (110) surface. Thus Cr segregation in Fe-Cr is a surface-facet specific property. We lend insight into the mechanism underlying the starkly suppressed surface layer relaxation determined for both these surfaces. The remainder of the paper is organized as follows. We briefly describe the theoretical background as well as methodological and computational details in Sec. II. In Sec. III, we present and discuss our main results on the surface energies and surface segregation energies of chemically homogeneous and chemically inhomogeneous Fe-Cr alloys, as well as the implication of these findings for the surface alloy phase diagram. We clarify the stability of the Cr surface magnetic moments against bulk Cr content on the basis of the surface electronic structure. Section IV concludes.

II. METHODOLOGY AND COMPUTATIONAL METHOD

A. Theoretical background

The surface energy $\gamma(x_b)$ for chemically homogeneous $Fe_{1-x_b}Cr_{x_b}$ alloys, defined as the energy cost of creating new surface area [23], may be extracted from slab calculations, viz.

$$\gamma = \frac{E_{\rm slab} - n_m E_b}{2A}. \tag{1}$$

Here, $E_{\rm slab}(x_b)$ is the total energy of a slab composed of n_m atomic layers, $E_b(x_b)$ is the bulk energy per layer, and $A(x_b)$ denotes the surface area for one of the two (identical) surfaces of the slab. Slabs of different thicknesses were employed in order to determine the bulk reference energy [24], i.e., the slope of a linear function fitted to $E_{\rm slab}$ versus n_m equals E_b (the correlation is linear for decoupled surfaces corresponding to sufficiently large n_m).

In the present application, the chemical composition of the surface is variable and may differ from the nominal bulk composition. The determination of surface segregation energies and surface energies of such chemically inhomogeneous systems requires knowledge of bulk and surface effective chemical potentials (ECPs). Similar to earlier work [18,25], the bulk is assumed to provide an infinite particle reservoir, and the ECP of the host is defined as the energy change per atom, when a Cr atom is exchanged with an Fe atom, viz.

$$\Delta\mu = \mu_{\rm Fe} - \mu_{\rm Cr}. \tag{2}$$

The ECP of random alloys may be obtained by means of its intensive definition [13], which for the bulk equals

$$\Delta\mu_b(x_b) = -\left(\frac{dE_b}{dx_b}\right)_a. \tag{3}$$

During this exchange the lattice parameter a remains constant. Similarly, we define the surface ECP $\Delta\mu_s(x_s; x_b)$ of a slab, when this atomic exchange takes place within the surface layers,

$$\Delta\mu_s(x_s; x_b) = -\frac{1}{2}\left(\frac{dE_{\rm slab}(x_s; x_b)}{dx_s}\right)_{a,d_{ij}}. \tag{4}$$

Here, x_s denotes the concentration of the surface alloy $Fe_{1-x_s}Cr_{x_s}$ in both surface layers, the concentrations of all the other layers in the slab equal the nominal bulk concentration x_b (the factor 1/2 associates μ_s with one surface layer). The interlayer distances d_{ij} are functions of x_s but are kept constant when determining the derivative (in addition to a). It should be noted that our notation simplifies to $E_{\rm slab}(x_b) \equiv E_{\rm slab}(x_b; x_b)$, and a similar convention is used for the surface energies, ECPs, and segregation energies.

The surface segregation energy $E_{\rm segr}(x_s; x_b)$ equals the energy change due to atomic exchange between the bulk and the

surface [13,16],

$$E_{\rm segr} = \frac{1}{2}\left(\frac{dE_{\rm slab}(x_{\rm s};x_{\rm b})}{dx_{\rm s}}\right)_{a,d_{ij}} - \left(\frac{dE_{\rm b}(x_{\rm b})}{dx_{\rm b}}\right)_{a} \quad (5a)$$

$$= -[\Delta\mu_{\rm s}(x_{\rm s};x_{\rm b}) - \Delta\mu_{\rm b}(x_{\rm b})]. \quad (5b)$$

In the present convention, moving a Cr atom from the bulk to the surface and simultaneously moving an Fe atom from the surface to the bulk is exothermic for negative $E_{\rm segr}$.

The surface energy of chemically inhomogeneous Fe-Cr alloys, assuming the surface alloy $Fe_{1-x_s}Cr_{x_s}$ at the two slab surfaces and $Fe_{1-x_b}Cr_{x_b}$ in the interior, may then be obtained from [13,26,27]

$$\gamma(x_{\rm s};x_{\rm b}) = \frac{E_{\rm slab}(x_{\rm s};x_{\rm b}) - n_m E_{\rm b}(x_{\rm b})}{2A} + \frac{\Delta\mu_{\rm b}(x_{\rm b})(x_{\rm s}-x_{\rm b})}{A}. \quad (6)$$

By comparing the derivative of Eq. (6) with respect to $x_{\rm s}$ and Eqs. (5), it is readily seen that

$$A\frac{d\gamma(x_{\rm s};x_{\rm b})}{dx_{\rm s}} \approxeq E_{\rm segr}, \quad (7)$$

if the relaxed interlayer distances do not strongly depend on $x_{\rm s}$.

We use the symbol Γ to represent the surface energy per atom in units of energy [i.e., not dividing by area in Eq. (1) or (6), or letting $\Gamma = \gamma A$], employed for convenience in the discussion part.

B. Methodological details

For both the chemically homogeneous and chemically inhomogeneous surface reference systems, slabs with 7, 9, and 11 atomic layers decoupled by vacuum corresponding to seven bulk inter-planar distances ($n_v = 7$) were determined sufficient to yield converged bulk and surface energies for the (110) surface. For the open (100) surface, the corresponding numbers are 11, 13, and 15 atomic layers, and $n_v = 7$. The relaxation of the interlayer spacing between the surface layer and the subsurface layer d_{12} into mechanical equilibrium [28] was considered (relaxation simultaneously performed at both slab surfaces) and determined from the slabs with $n_m = 11$ and $n_m = 13$ for the (110) surface and the (100) surface, respectively. The effect of relaxation was evaluated by comparison with perfectly truncated bulk slabs with the same thickness. It should be noted that surface reconstruction in Fe was not experimentally observed for either of these surface facets in the temperature range 300−500 K [29].

In order to allow for a possible antiferromagnetic alignment of Cr spins with respect to each other in the ferromagnetic Fe matrix, which is motivated by the fact that the incommensurate magnetic ground state of bcc Cr is closely approximated by a Néel state [30], we examined the spin-alignment of the Cr spins for laterally extended 2×2 super cell in terms of the (110) oriented surface slabs for $Fe_{0.91}Cr_{0.09}$. Within the present random solid solution description of the alloy, all Cr magnetic moments were, however, found to align parallel with respect to each other and antiparallel to the Fe spins.

The surface ECPs were also determined from the 11 layers [(110) facet] and 13 layers [(100) facet] slabs. The bulk ECPs were determined from super cells in order to facilitate numerical error cancellation (numerical errors may arise due to, e.g., different Brillouin zone samplings). In practice, the n_v layers vacuum of the slabs were replaced by material resulting in a total thickness of 18 layers for the (110)-type bulk reference system and of 20 layers for the (100)-type bulk reference system, respectively. The concentration derivatives were obtained from a linear fit to seven total energies computed for the finite concentration changes $\Delta x_{\rm b} = 0,\ \pm 0.001,\ \pm 0.002,$ and $\pm\ 0.003$, and similar for $x_{\rm s}$.

C. Computational method

The spin DFT calculations were performed with the all-electron exact muffin-tin orbitals (EMTO) method [31–33]. The self-consistent calculations were carried out with the local-density approximation by Perdew and Wang [34] and the total energies were calculated with the generalized-gradient approximation by Perdew, Burke, and Ernzerhof [35] via the full charge density technique [36,37]. The chemical disorder was treated by means of the CPA [38,39]. Since the CPA solves a single-site impurity problem, it can not directly describe local concentration fluctuations and local lattice relaxation, implying that the present results are valid for random solid solution alloys on a rigid underlying crystal lattice. Although neutron-diffusive scattering and Mössbauer spectroscopy experiments [40,41] reported atomic short-range order (ASRO) for the nearest-neighbor coordination shell in bulk $Fe_{1-x_b}Cr_{x_b}$, $x_{\rm b} \leqslant 15$ at.%, the treatment of ASRO is beyond the scope of the present work. Since the surface energy is a surface excess, bulk contributions are expected to cancel to a large extent. To our best knowledge, ASRO near surfaces has not been investigated for Fe-rich Fe-Cr alloy hitherto.

The Brillouin zones for the (110) and the (100) surface subsystems were sampled by a $13 \times 33 \times 1$ and $13 \times 25 \times 1$ k-point meshes, respectively. For the determination of the bulk ECPs by supercells, the number of k points along the third direction was set to two. All spin-polarized calculations were carried out for collinear magnetic configurations describing the energetics of the alloy well [20–22].

The precision of the EMTO method was demonstrated for mechanical properties, electronic structure, and the surface energy of alloys [42–44], including the Fe-Cr binary [18,19,27,45]. The theoretical equilibrium lattice parameters of bcc Fe and Fe-Cr alloys (0–15 at.% Cr) determined by EMTO were already reported previously [46] and our results reproduce these data well. Thus we refer the reader to Ref. [46] for further details.

III. RESULTS AND DISCUSSION

A. Surface energies and surface relaxation of chemically homogeneous Fe-Cr alloys

We first present the main findings on the relaxed surface energies of the Fe-Cr alloys and then briefly turn to the surface relaxation. The former are subject to further discussion in Sec. III D and the latter in Sec. III E.

The calculated surface energies $\gamma_{(100)}$ and $\gamma_{(110)}$ of chemically homogeneous $Fe_{1-x_b}Cr_{x_b}$ alloys, $0 \leqslant x_{\rm b} \leqslant 15$ at.%, are shown in Fig. 1. Focusing on the spin-polarized results

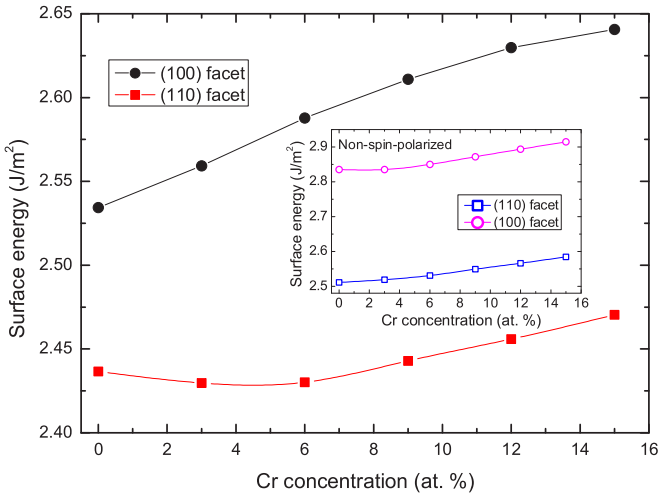

FIG. 1. The relaxed surface energies for the (100) and (110) surfaces of chemically homogeneous Fe-rich $Fe_{1-x_b}Cr_{x_b}$ alloy as a function of bulk concentration x_b. Results of spin-polarized calculations (main figure) and non-spin-polarized calculations with identical geometry (inset) are shown. Lines are a guide for the eye.

first, $\gamma_{(100)}$ increases monotonically with the addition of Cr by 0.11 J/m^2 for $\Delta x_b = 15$ at.% Cr, which is consistent with the previous theoretical results from Ref. [27]. In contrast, $\gamma_{(110)}$ is convex in x_b and has a local minimum at $x_b \approx 4$–5 at.% Cr. $\gamma_{(110)}$ is lower than $\gamma_{(100)}$ in the entire considered concentration range meaning that the (110) surface is more stable.

The present surface energies of ferromagnetic Fe are 2.53 and 2.44 J/m^2 for the (100) and the (110) surfaces, respectively. These values are consistent with literature data, i.e., Punkkinen *et al.* [47] recently computed 2.50 and 2.45 J/m^2, respectively, and Błoński and Kiejna [48] earlier reported 2.47 and 2.37 J/m^2, respectively. Our results agree well with the semi-empirical, low-temperature estimates of the surface energy for an average surface facet, which were derived from the experimentally determined surface tension, 2.41 J/m^2 (Ref. [49]) and 2.48 J/m^2 (Ref. [50]). Furthermore, we note that the anisotropy ratio $\gamma_{(100)}/\gamma_{(110)} = 1.04$ for Fe coincides with the experimental value 1.02 ± 0.06 derived from the high-temperature equilibrium shape of α-Fe crystallites [51]. Although these values were determined at different temperatures, recent theoretical work for Fe showed that $\gamma_{(100)}/\gamma_{(110)}$ is only weakly temperature dependent [52].

It is instructive to compare these results to those obtained without spin-polarization invoked in the calculations in order to highlight the effect of magnetism. The resulting data are shown in Fig. 1 (inset) and were obtained by keeping the interatomic distances fixed. Disabling spin polarization has two main effects: on the one hand, the surface energies of $Fe_{1-x_b}Cr_{x_b}$ generally increase. As this effect is more pronounced for the (100) surface, the anisotropy $\gamma_{(100)}/\gamma_{(110)}$ increases. For instance, $\gamma_{(100)}$ and $\gamma_{(110)}$ of nonmagnetic Fe amount to 2.84 J/m^2 (corresponding to a change of +0.31 J/m^2 relative to the spin-polarized results) and 2.51 J/m^2 (+0.07 J/m^2), respectively, and $\gamma_{(100)}/\gamma_{(110)} = 1.13$ (+0.09). On the other hand, the local minimum observed for the spin-polarized curve of $\gamma_{(110)}$ is removed and $\gamma_{(110)}$ becomes a monotonically increasing function of x_b. Thus magnetism plays an obviously important role in the formation of the local minimum of $\gamma_{(110)}$.

Turning briefly to surface relaxations, the spacings between the surface layer and the subsurface layer d_{12} of ferromagnetic bcc Fe were found to decrease by 1.33% for the (110) surface and 2.31% for the (100) surface. The available experimental data do not allow an unambiguous conclusion: 0.5%, 1.4 ± 3%, or 5 ± 2% for Fe(100), and 0% or 0.5 ± 2% for Fe(110) [29,53]. These findings confirm previous DFT investigations for pure Fe [47,48,54] reporting similar decreases of the surface energy, albeit relaxation of several layers were performed. Using the mean-field approximation (relaxing Fe and Cr on the same site simultaneously), we determined similarly small values and a weak dependence on composition in the case of the Fe-Cr alloys: d_{12} relaxes inward by 1.40%–1.46% and by 2.55%–2.78% for the (110) surface and the (100) surface, respectively. The decrease of the surface energy accompanying relaxation of d_{12} amounts to ≈1.3% for the (110) surface of Fe and ≈1.0% for the (100) surface of Fe. For the Fe-Cr alloys, the decrement of $\gamma_{(110)}$ lies in the interval of 1.3%–1.5% and that of $\gamma_{(100)}$ in the range of 1.2%–1.4%.

The amount of surface relaxation determined for Fe and Fe-Cr is in stark contrast to theoretical predictions for the nonmagnetic bcc transition metals (V, Nb, Mo, Ta, W) [55] and available experimental findings [29]. For these five elements, typically computed changes of spacing are $\Delta d_{12} \approx -(12$–$13)$% for the (100) facet and $\Delta d_{12} \approx -(4$–$5)$% for the (110) surface, reflecting a clear correlation with the surface roughness. The suppression of large relaxation effects in Fe and the ferrous alloys is attributed to the effect of surface magnetism and investigated in more detail in Sec. III E.

B. Surface segregation energies of chemically homogeneous Fe-Cr alloys

In order to give insight into the thermodynamic driving force of Cr segregation at the (100) and (110) surfaces, we consider the surface segregation energies for the chemically homogeneous alloys. The bulk and surface ECPs along with the surface segregation energies of pure Fe and three selected Fe-Cr binaries, $Fe_{0.97}Cr_{0.03}$, $Fe_{0.94}Cr_{0.06}$, and $Fe_{0.91}Cr_{0.09}$, are compared in Table I. (The ECPs of pure Fe are to be understood as removing a Cr impurity atom from the Fe matrix.) As is evident, the bulk ECP $\Delta\mu_b$ decreases with the addition of Cr, exhibiting a deviation from the linear rule of mixture. This behavior is closely related to the anomalous (i.e., negative and convex) bulk formation energy in Fe-rich Fe-Cr alloys [19,22], viz.

$$\frac{d^2 \Delta E_b(x_b)}{dx_b^2} \approx -\frac{d\Delta\mu_b}{dx_b}. \tag{8}$$

The bulk formation energy $\Delta E_b(x_b)$ is defined in Eq. (A1) (with $x_0 = 1$) in the Appendix and a plot of $E(x_b)$ can be found in Refs. [19,22]. According to Eq. (8), the convexity of $E_b(x_b)$ in the low-Cr regime follows the decreasing bulk ECP with increasing Cr content.

The key differences between the surface ECPs for the two considered surface facets are: the trend of $\Delta\mu_{s(110)}$ closely

TABLE I. Bulk ECP ($\Delta\mu_b$), surface ECPs ($\Delta\mu_s$), and surface segregation energies (E_{segr}) of Fe and chemically homogeneous $Fe_{0.97}Cr_{0.03}$, $Fe_{0.94}Cr_{0.06}$, and $Fe_{0.91}Cr_{0.09}$ alloys. $E_0 = -443.8$ Ry. All tabulated energies are in units of mRy.

	$\Delta\mu_b - E_0$	$\Delta\mu_{s(110)} - E_0$	$E_{segr(110)}$	$\Delta\mu_{s(100)} - E_0$	$E_{segr(100)}$
pure Fe	− 12.4	− 11.8	− 0.7	− 29.7	17.2
			7.3 (Ref. [13])		11.8 (Ref. [13])
			− 0.07 (Ref. [15])		5.6 (Ref. [15])
					9.6[a], 6.8[b] (Ref. [14])
					16.9 (Ref. [19])
					5.7 (Ref. [16])
					15.9[c] (Ref. [56])
$Fe_{0.97}Cr_{0.03}$	− 19.8	− 21.8	1.9	− 34.0	14.2
$Fe_{0.94}Cr_{0.06}$	− 33.5	− 35.2	1.7	− 38.2	4.7
$Fe_{0.91}Cr_{0.09}$	− 47.2	− 48.3	1.1	− 42.2	− 5.0

[a]EMTO value taken (theoretical lattice parameter, local-density approximation).
[b]Projector-augmented wave value for lowest effective Cr concentration taken (theoretical lattice parameter, generalized-gradient approximation, no relaxation).
[c]Value for 12 atomic layers taken.

resembles that of $\Delta\mu_b$, resulting in a small segregation energy $E_{segr(110)}$ not exceeding 2 mRy. This comparatively small energy indicates a tendency to Cr depletion from the surface for the case $x_s = x_b$, i.e., a weak driving force for desegregation, except for the pure Fe host. $\Delta\mu_{s(100)}$ exhibits a stronger concentration dependence involving a change of sign of $E_{segr(100)}$ between 6 and 9 at.% bulk Cr content. That is, for the chemically homogeneous (100) surface slabs, we find both a tendency to Cr segregation to the bulk below a certain bulk threshold concentration (in between 6 and 9 at.% Cr) and Cr segregation to the surface above this threshold. Ropo *et al.* [18] narrowed down the critical bulk Cr concentration at which the transition occurs to ≈9 at.%.

The available literature data of Cr segregation energies in pure Fe listed in Table I allow comparison with the present values. They were obtained from either single-atom segregation studies [14–16] or by means of the CPA [13,14,19,56]. It should be noted that the tabulated literature values are those derived for the lowest effective Cr concentration (corresponding to the largest employed super cells) if multiple values were reported. For the Fe(110) surface, all segregation energies are consistent in sign, indicating Cr depletion from the surface, but vary considerably in absolute value. The CPA values except that from Ref. [14] are approximately a factor of 2–3 times larger than the segregation energies from the single-atom segregation studies. These differences are likely due to methodology, e.g., finite-size effects in the single-atom segregation studies, the fact that the ordered lattice of effective potentials contains Cr on each site in the CPA treatment, as well as local lattice relaxation effects. The slightly negative $E_{segr(110)}$ determined here qualitatively supports the finding from Kiejna and Wachowicz [15].

C. Surface energies of chemically inhomogeneous Fe-Cr alloys

The main results of this section are the surface energies $\gamma(x_s; x_b)$ of chemically inhomogeneous Fe-Cr alloys and implications for the surface alloy phase diagram. These results were obtained without taking the relaxation of d_{12} into account, which is justified first.

Figure 2 compares the surface energies of the (110) and (100) surfaces for the nominally 9 at.% bulk Cr containing Fe-Cr binary with and without top layer relaxation. The Cr concentration at the surface was varied within $0 \leqslant x_s \leqslant 15$ at.% in these and the following calculations. As can be seen, the effect of relaxation on $\gamma_{(110)}$ is a decrease of approximately 0.036 J/m^2 (or ≈1.5%) nearly independent on x_s. A similar, but slightly more strongly concentration-dependent decrement was determined for $\gamma_{(100)}$: the decrease lies between 0.032 J/m^2 (≈1.2%) and 0.040 J/m^2 (≈1.5%). That is, both curves are essentially shifted upon relaxation by a nearly constant amount leaving the shape of curve invariant (this also implies that the surface ECPs $\Delta\mu_s(x_s; x_b)$ are nearly invariant). The relaxation of d_{12} can thus justifiably be neglected as the primary interest is in the trend of $\gamma(x_s; x_b)$ as a function of x_s. The following results were obtained with this approximation.

Figure 3 shows the relationships between the unrelaxed surface energies of the (100) and (110) surfaces versus x_s for the nominal bulk compositions $Fe_{0.97}Cr_{0.03}$, $Fe_{0.94}Cr_{0.06}$,

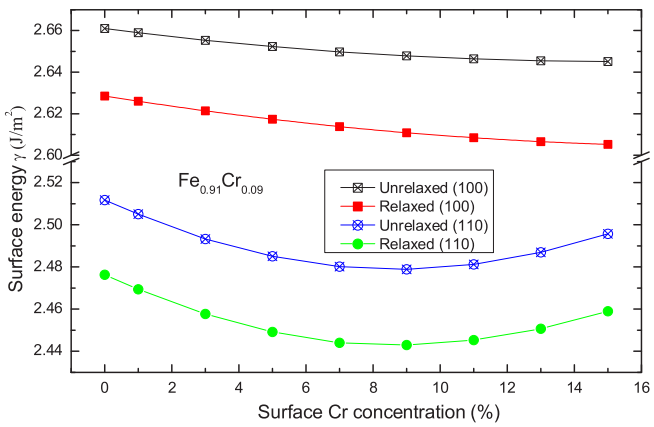

FIG. 2. Surface energies for the (100) and (110) surfaces with and without considering relaxation of d_{12} as a function of surface Cr concentration x_s for the nominal bulk composition $Fe_{0.91}Cr_{0.09}$. Lines are a guide for the eye.

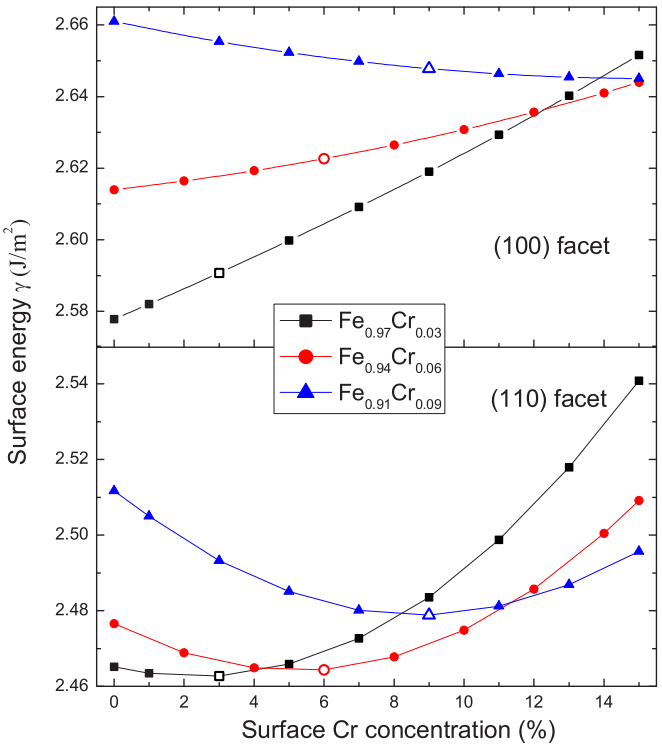

FIG. 3. Unrelaxed surface energies for the (100) and (110) surfaces as a function of surface Cr concentration x_s for the Fe-Cr binaries with nominal bulk Cr concentration x_b of 3, 6, or 9 at.%. The open symbols highlight chemically homogeneous alloys ($x_s = x_b$). Lines are a guide for the eye.

and $Fe_{0.91}Cr_{0.09}$ (data for $Fe_{0.91}Cr_{0.09}$ are the same as the unrelaxed values from Fig. 2). We highlight several trends in $\gamma(x_s;x_b)$: $\gamma_{(100)}$ of bulk $Fe_{0.97}Cr_{0.03}$ and $Fe_{0.94}Cr_{0.06}$ increase with Cr surface concentration, whereas that of $Fe_{0.91}Cr_{0.09}$ reduces and all three curves are slightly convex. The $\gamma_{(110)}$ curves are convex functions in x_s for all three considered bulk compositions. The common shape of the curves signals that the lowest (110) surface energy on each curve lies within ± 1 at.% Cr vicinity of the homogeneous concentration profile. Strictly speaking, since $E_{segr(110)} \gtrapprox 0$ (Sec. III B), the minimizing x_s is smaller than x_b. We note in passing that Ref. [27] focused on $\gamma_{(100)}(x_s;x_b)$ for two intermediate bulk compositions, $Fe_{0.95}Cr_{0.05}$ and $Fe_{0.90}Cr_{0.10}$, and their computed trends are consistent with the present findings. It should also be noted that the curves in Fig. 3 appear to be similar in shape but shifted to lower x_s for higher x_b. This point is further analysed in Sec. III D.

The shape of the curves $\gamma(x_s;x_b)$ allows some insight into the surface equilibrium at low temperature by considering purely energetic contributions [57]. It should be noted that the surface equilibrium state may not be established instantly due to kinetic reasons as bulk diffusion at room temperature and below is usually very slow, which may lead to a quasiequilibrium surface state. On the one hand, by comparing $\gamma(x_s;x_b)$ with the rule of mixing for an ideal solid solution one can draw conclusions about the formation energy of the surface alloy. The surface formation energy is defined in the Appendix, Eq. (A5). We chose as reference points (standard states) a purely Fe terminated surface and the surface alloy with 15 at.% Cr, since the available data is limited to $x_s \leqslant 15$ at.%, that is, $x_0 = 0.15$ in Eq. (A5). On the other hand, the minimum of $\gamma(x_s;x_b)$ (over all x_s) provides information about the surface alloy composition in equilibrium when surface segregation is taken into account. It should be noted that the minimizing surface energy does not need to coincide with $d\gamma(x_s;x_b)/dx_s = 0$. This is the case for the (100) terminated slab and two bulk compositions shown in Fig. 3 as $d\gamma(x_s;x_b)/dx_s$ is finite when x_s approaches zero. In contrast, the minimum of $\gamma(x_s;x_b)$ coincides with its vanishing first derivative with respect to x_s for the (110) surface.

With respect to these two reference concentrations, the convexity of all surface energy curves $\gamma(x_s;x_b)$ shown in Fig. 3 indicates that the formation of a surface solid solution is energetically favorable over phase separation into islands. For the (100) surface, $E_{segr}(x_s;x_b)$ is positive when x_b equals 3 or 6 at.% and a purely Fe terminated surface layer possesses the lowest surface energy. Thus, all Cr would segregate from the surface to the bulk and dissolve. In contrast, a Cr enriched surface ($x_s > 15$ at.%) has the lowest surface energy for $x_b =$ 9 at.% indicating Cr segregation to the surface (Ropo *et al.* determined that $E_{segr} = 0$ for $x_s \approx 24$ at.% [18], i.e., above the presently considered upper limit on x_s). For the (110) surface, the minimum of the surface energy close to a homogeneous concentration profile indicates that practically any surface excess of Cr or Fe would segregate to the bulk in order to reach the lowest energy state at $x_s \approxeq x_b$. In other words, Cr does not have a favorable site among the two considered subsystems. For both facets, configurational entropy is expected to homogenize the concentration profiles at finite T.

D. Formation energies

The surface energies of the chemically homogeneous and inhomogeneous Fe-Cr alloys shown in Figs. 1 and 3 exhibit different alloying trends. For instance, $\gamma_{(100)}$ of the homogeneous system increases with increasing Cr concentration similar to the variation of the inhomogeneous systems for the nominal bulk compositions $Fe_{0.97}Cr_{0.03}$ and $Fe_{0.94}Cr_{0.06}$. On the other hand, $\gamma_{(100)}$ decreases with x_s for $Fe_{0.91}Cr_{0.09}$. Previous works focused on explaining the anomalous bulk formation energy of the Fe-Cr binary using electronic structure arguments [19,22]. Here, we make an attempt to understand the trends in the computed surface energies and thus the surface alloy phase diagram of the inhomogeneous alloys starting from the results obtained for the homogeneous surface slabs and the bulk alloys. To this end, we introduce a simple model that represents the total energy of the slab as a sum of a surface layer contribution denoted by $\bar{E}(x_s)$ and a bulk contribution. In the case of homogeneous slabs, the definition of $\bar{E}(x_s)$ is given in Eq. (A6). Assuming a similar surface layer contribution for the inhomogeneous surface, the total energy of the inhomogeneous slab contains an "interfacial" contribution $\sigma(x_s;x_b)$ in addition. This excess energy accounts for the interaction between the surface layer with composition x_s and the subsurface layers with composition x_b, as well as the small volume effect originating from the concentration dependence of the equilibrium volume. The definition of

$\sigma(x_s; x_b)$ is given in Eq. (A7). In the following, we assume that the interfacial term is small and discuss the formation energies and surface energies of the two types of slabs.

First, we compare the formation energies of homogeneous and inhomogeneous slabs for identical surface composition x_s but different nominal bulk Cr concentration (i.e., the slab interior). Not considering the interfacial term in Eq. (A8) leads to the following approximation for the difference between the formation energies of the homogeneous and inhomogeneous slabs,

$$\Delta E_{\text{slab}}(x_s) - \Delta E_{\text{slab}}(x_s; x_b) \approx (n_m - 2)\Delta E_b(x_s). \quad (9)$$

This formula expresses the fact that the formation energy of the inhomogeneous slab $\Delta E_s(x_s; x_b)$ is defined for the surface layers only, i.e., there is no contribution coming from the $(n_m - 2)$ internal layers. On account of the considered Cr concentration interval, we chose as reference states pure Fe and $Fe_{0.85}Cr_{0.15}$ to derive the formation energies. We selected $x_b = 0.06$ in order to compute $\Delta E_s(x_s; x_b)$ (the results for other x_b values are similar) and computed the left- and right-hand sides of Eq. (9) as a function of x_s. Slabs with n_m equal to 11 atomic layers and 13 atomic layers for the (110) surface and the (100) surface, respectively, were chosen.

The three formation energy terms appearing in Eq. (9) are shown in Fig. 4 along with the difference between the two slab formation energies [left-hand side of Eq. (9)]. This differences agrees reasonably well with the right-hand side of Eq. (9) establishing the accuracy of the approximation; the deviations are due to the neglected interfacial term. An explicit evaluation of σ and $\Delta\sigma$ using Eqs. (A7) and (A9) resulted in $\sigma(0; 0.06) = 0.71$ meV, $\sigma(0.06; 0.06) = 0.0$ meV, and $\sigma(0.15; 0.06) = -16.48$ meV for the (110) surface, and $\sigma(0; 0.06) = 27.11$ meV, $\sigma(0.06; 0.06) = 0.0$ meV, and $\sigma(0.15; 0.06) = -34.20$ meV for the (100) surface. Further evaluation gave $2\Delta\sigma_{(110)}(0.06; 0.06) = 14.04$ meV and $2\Delta\sigma_{(100)}(0.06; 0.06) = -5.17$ meV. These values for $\Delta\sigma(x_s; x_b)$ are identical to the differences between the left- and right-hand sides of Eq. (9) as plotted in Fig. 4. This intermediate result shows that the formation energies of the two slabs basically differ by the bulk formation energy weighted with the number of subsurface layers. In the following, we turn to the surface energies assuming again that the sigma term is small.

In order to understand the different surface alloying effects on the surface energies of the chemically inhomogeneous Fe-Cr system with fixed bulk concentration and the chemically homogeneous Fe-Cr alloy, we rewrite Eq. (A7) using the surface energies in units of energy (Γ), viz.

$$\Gamma(x_s; x_b) - \Gamma(x_s) = E_b(x_s) - E_b(x_b) + \Delta\mu_b(x_b)(x_s - x_b) + \Delta\sigma(x_s; x_b). \quad (10)$$

We then take the derivative of this expression with respect to the surface concentration x_s dropping the $\Delta\sigma$ term,

$$\frac{d\Gamma(x_s; x_b)}{dx_s} - \frac{d\Gamma(x_s)}{dx_s} \approx \frac{dE_b(x_s)}{dx_s} + \Delta\mu_b(x_b). \quad (11)$$

This relationship expresses the fact that the slopes of the two surface energies versus surface concentration differ from each other by a term that depends merely on bulk quantities. We

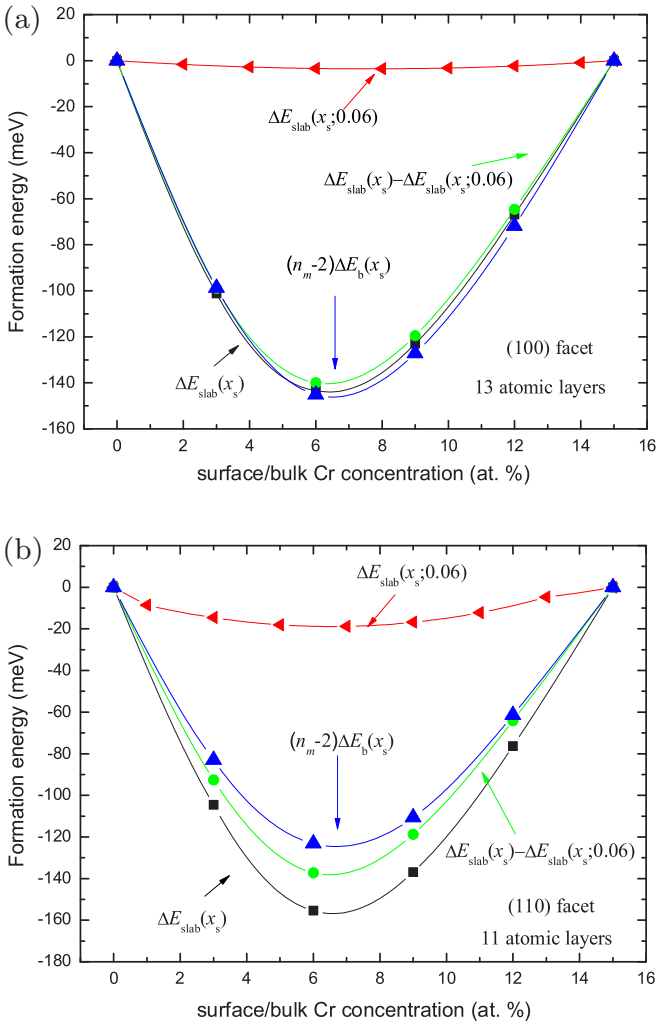

FIG. 4. The relationship between the bulk formation energy, the formation energies of chemically homogeneous slabs and inhomogeneous slabs (with $x_b = 0.06$ in the interior) and their difference according to Eq. (9) as a function of surface or bulk Cr concentration.

can easily verify Eq. (11) by taking the slopes in the limit of low x_s and considering a low x_b of 0.03. The right-hand side of Eq. (11) nearly vanishes in this case (apart from the volume effect) and thus the two surface energy terms should exhibit similar derivatives against x_s. Indeed, Figs. 1 and 3 show a qualitative agreement between the compositional effect of Cr on the surface energy of the chemically inhomogeneous slabs for low-x_s and chemically homogeneous slabs for low x_b.

Equation (11) also suggests that the difference in the slopes of the surface energy depends on the bulk concentration mainly through a bulk contribution. Taking the derivative of Eq. (11) with respect to x_b gives

$$\frac{d^2\Gamma(x_s; x_b)}{dx_b dx_s} \approx \frac{\Delta\mu_b(x_b)}{dx_b}. \quad (12)$$

That is, the bulk concentration effect on the slope of the surface energy of the inhomogeneous alloy equals approximately the second-order derivative of the bulk energy (with negative sign). Since the second-order derivative of the bulk energy at constant volume is relatively close to the second-order

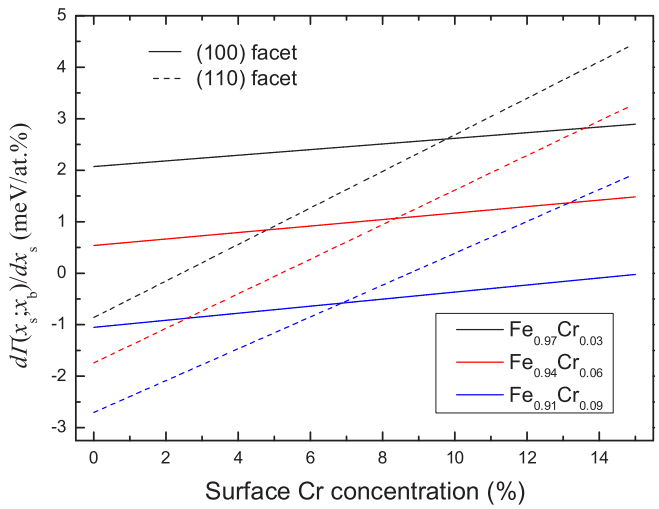

FIG. 5. The first-order derivative of $\Gamma(x_s;x_b)$ with respect to x_s plotted as a function of surface Cr concentration for the (110) and (100) surface terminations of chemically inhomogeneous Fe-Cr alloys and varying bulk Cr content as indicated in the legend.

derivative of the formation energy, which in the case of Fe-rich Fe-Cr alloys has a positive curvature (cf. discussion in Sec. III B), we expect that $-d^2E_b(x_b)/dx_b^2$ should be negative for $x_b \lessapprox 0.15$. Increasing x_b should thus decrease the slopes of the surface energies and the decrease should be of similar magnitude for both surfaces. To verify this, we computed the derivatives of the surface energies from Fig. 3, represented in units of energy, with respect to x_s after fitting to second-order polynomials. From the results shown in Fig. 5, we find that the derivatives are indeed shifted to smaller values, by an amount that weakly depends on x_s, as x_b increases. For instance, the differences between the curves for $Fe_{0.97}Cr_{0.03}$ and $Fe_{0.94}Cr_{0.06}$ amount to ≈0.3 and ≈0.5 meV/at.% for the (110) surface and the (100) surface, respectively. These values are consistent with the variation of the bulk ECP as a function of x_b [right-hand side of Eq. (12)] evaluated using the data from Table I. The similarity is due to the identical bulk and thus the change in the slope as a function of x_b does not depend on the surface termination. Figure 5 confirms our initial assumption that the change in the slope of the surface energies for the inhomogeneous surfaces against bulk concentration has a bulk origin [Eq. (12)]. We conclude that the complex behavior of the surface energies of the inhomogeneous slabs shown in Fig. 3 is primarily due to the underlying bulk effect rather than an influence of the surface.

E. The role of magnetism in the suppressed layer relaxation of chemically homogeneous Fe-Cr alloys

The purpose of this section is to explain the suppressed surface layer relaxation in Fe-Cr alloys using the resolved magnetic moments in the bulk and near the surface.

The employed mean-field alloy theory yields Cr spin magnetic moments aligned anti-parallel to the Fe moments of the host (assigned positive signs). The bulk magnetic moments m_b of Fe are stable against Cr concentration, whereas the Cr magnetic moments gradually increase, i.e., from -1.63 to $-0.89\ \mu_b$ when x_b increases from 0 to 15 at.%, see Fig. 6 (all Cr impurity level calculations done with $x = 0.05$ at.%).

We also present the species resolved magnetic moments in the surface layer m_s (for which the deviations from the bulk values are the largest) for chemically homogeneous Fe-Cr alloys in Fig. 6. For both the Fe and Cr species, the absolute surface magnetic moments are enhanced and this effect is obviously more pronounced for the open (100) surface. At the impurity level, the Cr magnetic moments amount to $-3.06\ \mu_b$ and $-2.54\ \mu_b$ for the (100) and the (110) surfaces, respectively. The Fe surface magnetic moments exhibit a weak concentration dependence similarly to the bulk. The Cr surface magnetic moments at both surface facets are, however, significantly more stable than their bulk counterparts. We draw upon the surface electronic structure of the Fe-Cr alloy in Sec. III F to explain the enhancement and stability of the Cr surface moments. We note in passing that the experimental magnetic moment of a complete Cr monolayer grown on Fe(100) was found to be of the same magnitude, i.e., $\approx 3\ \mu_b$ per site (no information on possible surface alloying was provided) [58].

As pointed out in Sec. III A, the top-layer relaxations for the (110) and (100) surfaces of Fe and Fe-Cr are significantly smaller than the values typically predicted for the nonmagnetic bcc transition metals. We show in the following that this is due to the magnetic contribution to the total stress responsible for the surface layer relaxation into mechanical equilibrium. This magnetic surface layer relaxation stress is closely related to the concept of bulk magnetic pressure [59,60] and magnetic surface stress [54] of the in-plane components of the surface stress tensor.

Let the cleaved surface be located in the plane defined by $z = \text{const}$. We define the surface layer relaxation stress normal to the surface and corresponding strain as

$$\tau_{zz} = \frac{1}{A}\frac{\partial E}{\partial \epsilon_{zz}} \quad \text{and} \quad \epsilon_{zz} = \frac{d_{12} - d_{12}^0}{d_{12}^0}, \tag{13}$$

respectively, where d_{12}^0 is the relevant bulk interlayer distance in equilibrium. τ_{zz} has the units J/m^2 similar to the interfacial excess stress [23]. Let $\tau_{zz}^0 \equiv \tau_{zz}(\epsilon_{zz} = 0)$ be the value for the perfectly truncated bulk.

In order to understand the role of surface magnetism in the observed surface relaxation behavior we performed additional fixed spin-moment calculations of the surface-layer relaxation for pure Fe and $Fe_{0.91}Cr_{0.09}$. In Fig. 6(b), we plot the strain ϵ_{zz} corresponding to mechanical equilibrium as a function of the stress τ_{zz}^0 for a series of surface magnetic moments m_s kept fixed during relaxation. Several interesting conclusions may be drawn. Firstly, Fig. 6(b) makes evident that the top layer relaxation and τ_{zz} are to a good approximation linearly related for both considered surfaces of bcc Fe and $Fe_{0.91}Cr_{0.09}$. The slopes determined for Fe by linear interpolation of the data are -0.86 and -0.30 $(J/m^2)^{-1}$ for the (100) and the (110) surfaces, respectively. The corresponding slopes for $Fe_{0.91}Cr_{0.09}$ are similar. The linearity follows from the somewhat surprising fact that the stiffness of the layer relaxation $\propto \partial^2 E/\partial \epsilon_{zz}^2$ only weakly depends on the parameter m_s (higher-order terms in the strain turned out to be negligible). Reducing the magnitude of the surface magnetic moments leads to a

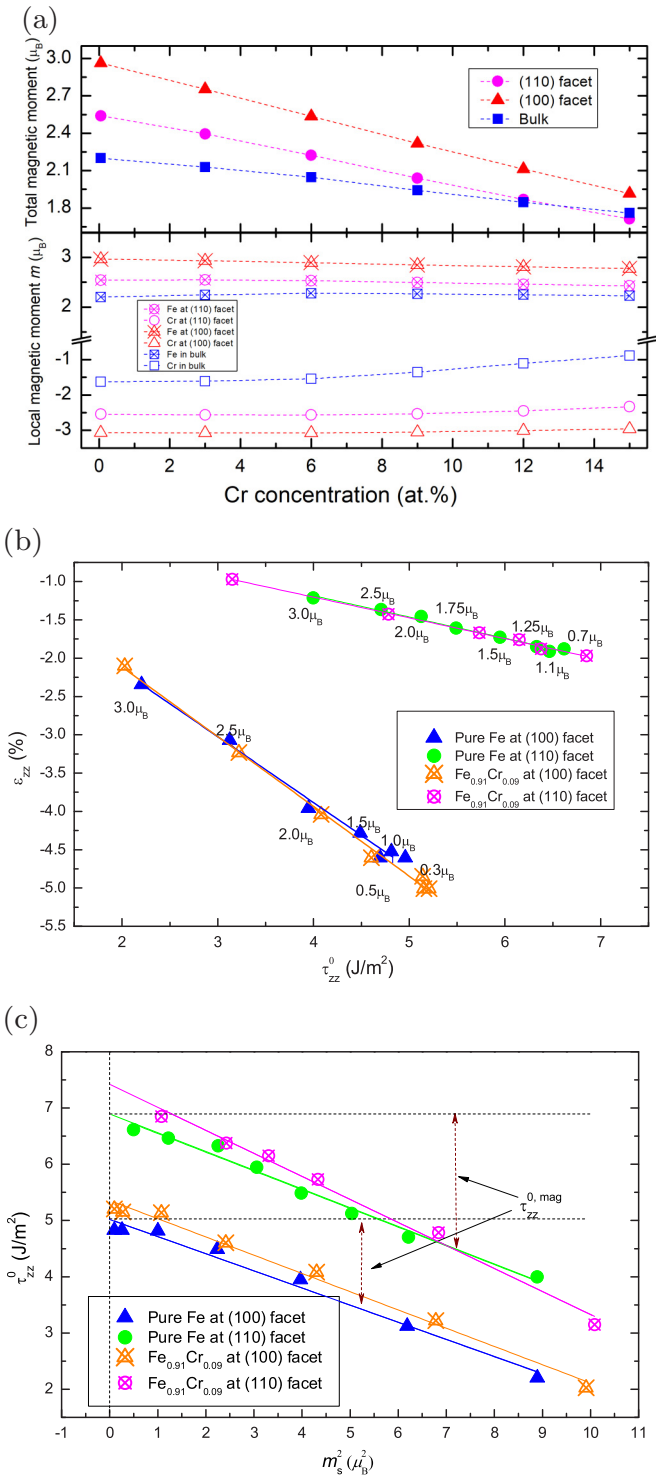

FIG. 6. (a) The total and species resolved magnetic moments for chemically homogeneous $Fe_{1-x_b}Cr_{x_b}$ alloys in the bulk and at the (100) and (110) surface facets (impurity level calculations carried out for 0.05 at.%; lines are a guide for the eye). For Fe and $Fe_{0.91}Cr_{0.09}$, (b) the correlation between the surface layer relaxation strain ϵ_{zz} and the surface layer relaxation stress τ^0_{zz}, wherein the surface magnetic moments m_s denoted in the figure refer to Fe; (c) the correlation between τ^0_{zz} and m_s^2, wherein the magnetic contribution $\tau^{0,mag}_{zz}$ is indicated for Fe. The solid lines in (b) and (c) interpolate the data.

larger inward relaxation of d_{12}. Since this effect is more pronounced for the open (100) surface facet, the relaxations of d_{12} for the smallest considered m_s exhibit a correlation with the surface roughness that is reminiscent of the nonmagnetic bcc transition metals as mentioned above. Nevertheless, the absolute values of d_{12} (for the smallest m_s) are somewhat smaller than those of the nonmagnetic bcc metals, which is likely due to electronic structure differences as well as the influence of the spin-polarized subsurface layers in the present calculations.

Secondly, the relationship between τ^0_{zz} and m_s is nonlinear; see Fig. 6(b). Let the total stress τ^0_{zz} be a sum of a regular contribution and a magnetic contribution, i.e., $\tau^0_{zz} = \tau^{0,reg}_{zz} + \tau^{0,mag}_{zz}$, where the regular contribution is the one of a non-spin-polarized surface layer $[\tau^0_{zz}(m_s = 0)]$ and the magnetic contribution is defined as the difference in stress between the spin-polarized calculations with m_s and the non-spin-polarized calculations. Then, we find that a close approximation of $\tau^{0,mag}_{zz}$ is provided by a quadratic dependence on m_s, viz.

$$\tau^{0,mag}_{zz} \propto \kappa_{(hkl)} m_s^2, \tag{14}$$

as shown in Fig. 6(c). $\kappa_{(hkl)}$ is a surface facet specific slope. By data interpolation [solid lines in Fig. 6(c)], $\kappa_{(100)}$ and $\kappa_{(110)}$ were determined to -0.28 and -0.33 J m^{-2} μ_b^{-2}, respectively, in the case of Fe. By means of extrapolating these lines to $m_s = 0$, $\tau^{0,reg}_{zz}$ amounts to $\approx$7 and $\approx$5 J/m^2 for the (110) and the (100) surfaces, respectively. The corresponding data for $Fe_{0.91}Cr_{0.09}$ are relatively similar. Obviously, the magnetic stress component is compressive and favors outward relaxation.[1]

A square dependence of the magnetic stress on the surface moment similar to Eq. (14) was previously reported for the in-plane components of the surface excess stress [52,54]. In contrast to the normal component considered here, the in-plane components cause practically no strain in the material except in nanocrystals [61]. The origin of the square dependence of the magnetic pressure was explained within the canonical theory of d bands and in the Stoner model for magnetism [59,60].

The above discussion considered the effect of spin-polarization on the layer relaxation; it included the spontaneously spin-polarized long-range-ordered magnetic state and the non-spin-polarized (nonmagnetic) state as special cases. A simple and direct means of assessing whether the electronic spin polarization of the electronic structure is important and/or the presence of long-range magnetic order is achieved if a paramagnetic state is considered. To this end, we drew upon the alloy analogy of the disordered local moment model for the paramagnetic state [62,63], which yields similar magnitudes of the local magnetic moment for the ferromagnetic and paramagnetic states of bcc Fe ($\approx$2.1–2.2 μ_b). The effect of long-range magnetic order versus random directional disorder can thus be directly assessed by way of comparing the layer relaxation. For both paramagnetic Fe and $Fe_{0.91}Cr_{0.09}$ at

[1]Convention: for positive or tensile (negative or compressive) stress, the bulk or surface would like to contract (expand).

their theoretical equilibrium volumes, we obtained an inward relaxation of 1.6% and 2.5% for the (110) facet and the (100) facet, respectively. These figures are very similar to those computed for magnetically ordered Fe and $Fe_{0.91}Cr_{0.09}$ (Sec. III A), indicating that the local electronic spin polarization of the electronic structure plays a more important role in the top-layer relaxation of Fe and the Fe-rich Fe-Cr binary than magnetic long-range order. This result is consistent with a previous investigation of the surface stress at the (110) and (100) facets of bcc Fe in ferromagnetic and paramagnetic states [52].

F. Electronic structure

In order to understand the electronic origin of the enhanced surface magnetic moments and the stability of the Cr surface magnetic moments against composition, we analyze the densities of states (DOSs) at the two surface facets in comparison to the bulk DOS for Fe and chemically homogeneous Fe-Cr alloys with $x_b = 0.03,\ 0.09,$ and 0.15.

The bulk DOS of bcc Fe shown in Fig. 7(a) exhibits the characteristic three-peak structure formed by the T_{2g} and E_g scalar d orbitals in both spin channels. The Fermi level resides near the bottom of the pseudogap in the minority spin channel, roughly separating bonding from antibonding states, and at the T_{2g} shoulder of the majority band. Bulk Cr is also exchange split with similar d band width to Fe, but favors antiferromagnetic order (for a plot of the bulk and surface DOSs of Cr, we refer to Refs. [30,64]). The band center of the Fe minority spin states and the band center of the Cr majority spin states are close in energy relative to their common d band width and align in the Fe-rich alloy to form a "common-band"-like minority spin band [65].

Due to the different exchange splittings of Fe and Cr, the majority spin electron DOS of the alloy shows pronounced split-band behavior; see Fig. 7(a). This is evident from the antibonding, Lorentzian-type virtual bound state (VBS) formed by the d states of Cr above the majority d states of Fe, and arises from hybridization effects [66]. Consequently, the Cr and Fe moments are aligned in opposite directions. Alloying with Cr generally smears out features of the DOS, the T_{2g} shoulder of Fe is pushed to below the Fermi level [67], and the Cr VBS broadens and becomes gradually occupied. This effect mainly causes the magnetic moment of Cr to decrease in magnitude with increasing its concentration; cf. Fig. 6(a). In contrast, the minority spin electron alloy DOS is virtually pinned at the Fermi energy (some spectral weight is shifted to above the Fermi energy in order to maintain the occupation number).

The surface atoms possess reduced coordination numbers and lower site symmetries narrowing the valence band width and partially or totally removing the typical three-peak structure in the surface DOS; see Figs. 7(b) and 7(c). Overall speaking, the total DOS at the close-packed (110) surface resembles the bulk one more closely, which is plausible from the fewer number of broken bonds. That is, in terms of a simple bond cutting model, two nearest neighbor (NN) bonds and two next-nearest neighbor (NNN) bonds are cut for a (110) surface atom, whereas four NN bonds and two NNN bonds are cut for a (100) surface atom. Moreover, the T_{2g} and E_g

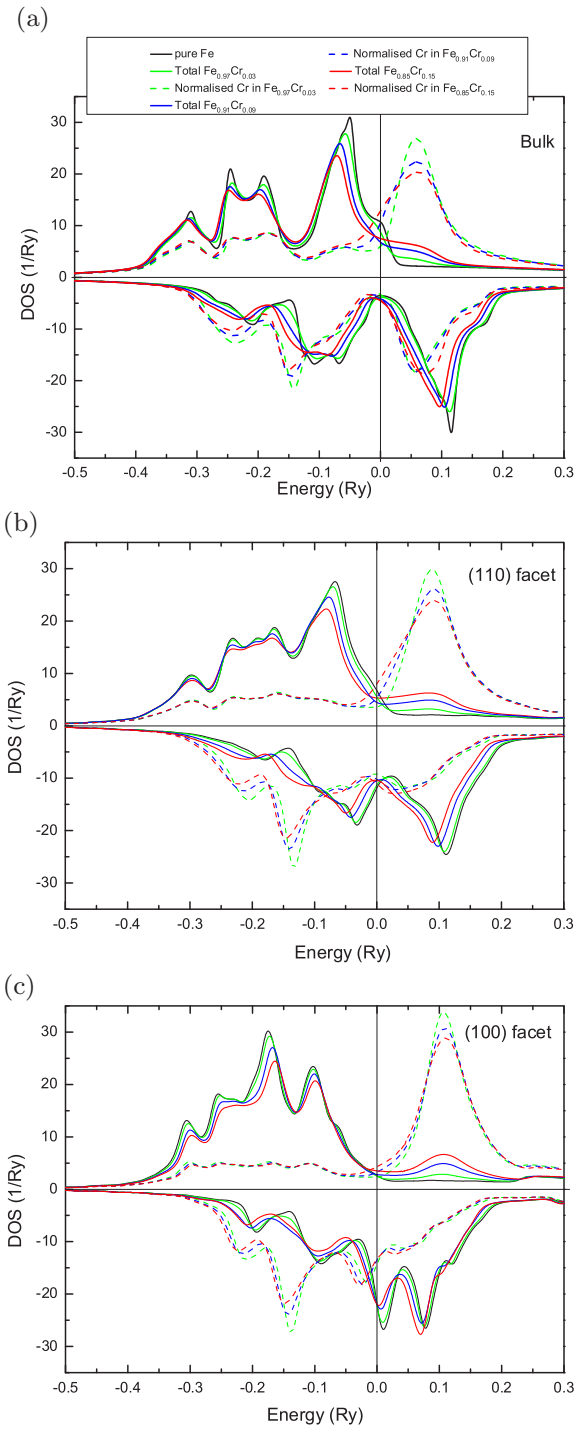

FIG. 7. DOS per atom for pure Fe and chemically homogeneous $Fe_{1-x_b}Cr_{x_b}$ random alloys ($x_b = 0.03,\ 0.09,\ 0.15$) for (a) the bulk, (b) at the (110) surface facet, and (c) at the (100) surface facet. The total DOS and the Cr resolved DOSs normalized to 100 at.% are shown (the Fe resolved DOSs are not shown as they approximate the total DOSs). The legend applies to all panels. The eigenenergies are plotted relative to the Fermi energy.

representations are lifted to five one-dimensional representations at the (110) surface, and one two-dimensional and three one-dimensional representations at the (100) surface. For both alloy surfaces, the Cr VBS is shifted to higher energies and

becomes narrower, indicating that the majority spin electron DOSs exhibit stronger split-band behavior than the bulk. The split-band behavior in the minority spin electron DOSs increases as well, which arises from the less well aligned surface minority spin states of Fe and the surface majority spin states of Cr in comparison to the bulk (recall, that Cr has a significantly enhanced surface magnetic moment). The significantly increased Cr surface magnetic moment in the Fe-rich alloys relative to its bulk value (Fig. 6) originates from this enhanced split-band behavior. The stability of the Cr surface magnetic moments at both surfaces against bulk composition follows from the fact that the VBS is pushed to higher energies, and only the lower-energy tails become occupied as the Cr concentration increases.

IV. CONCLUSIONS

We examined the compositional dependence of the surface energies and surface segregation energies of Fe-rich Fe-Cr alloy for the (100) terminated and (110) terminated surfaces through DFT simulations. We found that a threshold behavior of the surface Cr composition does not occur at the (110) surface. Instead, a surface alloy with Cr amount nearly equal to that of the bulk is energetically favorable for all nominal bulk Cr concentrations $\leqslant$15 at.%. In contrast, the surface chemistry of Fe-Cr(100) is characterized by Cr depletion (enrichment) at below (above) the critical bulk Cr composition window of 6–9 at.%. Thus the energetics of the Cr surface segregation in the Fe-Cr binary is surface-facet specific, which may lead to differences in the precipitation of Cr and ultimately the Cr oxide formation at these free surfaces.

We showed that the strongly suppressed surface-layer relaxation at both surfaces of the Fe-Cr alloys is of magnetic origin. Our results indicate that the local electronic spin polarization of the electronic structure is mainly responsible for this effect rather than the presence of long-range magnetic order. In particular, we provided evidence that the magnetic contribution (favoring outward relaxation) to the surface layer relaxation stress follows a dependence on the surface magnetic moment squared. This relationship should be verified for other surface facets and magnetic materials. The electronic origin for the higher stability of the Cr surface magnetic moments against bulk Cr content in comparison to the bulk case was clarified.

ACKNOWLEDGMENTS

This work was supported by the Swedish Research Council, the Swedish Foundation for Strategic Research, the Swedish Foundation for International Cooperation in Research and Higher Education, and the Hungarian Scientific Research Fund (research project OTKA 128229). The National Magnetic Confinement Fusion Program of China (2015GB118001) and the China Scholarship Council are acknowledged for financial support. The simulations were performed on resources provided by the Swedish National Infrastructure for Computing (SNIC) at the National Supercomputer Centre in Linköping.

APPENDIX: FORMATION ENERGY FORMULAS

Choosing as standard states bcc Fe and bcc $Fe_{1-x_0}Cr_{x_0}$, the bulk formation energy of the alloy $Fe_{1-x_b}Cr_{x_b}$, $0 \leqslant x_b \leqslant x_0$, may be derived from

$$\Delta E_b(x_b) = E_b(x_b) - \frac{x_0 - x_b}{x_0} E_b(0) - \frac{x_b}{x_0} E_b(x_0). \quad \text{(A1)}$$

Similarly, the formation energy of a chemically homogeneous slab may be expressed by

$$\Delta E_{slab}(x_b) = E_{slab}(x_b) - \frac{x_0 - x_b}{x_0} E_{slab}(0) - \frac{x_b}{x_0} E_{slab}(x_0). \quad \text{(A2)}$$

Subtracting the previous two equations for the same number of layers (n_m) yields the surface excess,

$$\Delta E_{slab}(x_b) - n_m \Delta E_b(x_b) = 2\Gamma(x_b) - \frac{x_0 - x_b}{x_0} 2\Gamma(0) - \frac{x_b}{x_0} 2\Gamma(x_0). \quad \text{(A3)}$$

Similar to Eq. (A2), we may express the formation energy for the surface alloy with concentration x_s, $0 \leqslant x_s \leqslant x_0$, and nominal bulk Cr concentration x_b through the energies of chemically inhomogeneous slabs, viz.

$$\Delta E_{slab}(x_s; x_b) = E_{slab}(x_s; x_b) - \frac{x_0 - x_s}{x_0} E_{slab}(0; x_b) - \frac{x_s}{x_0} E_{slab}(x_0; x_b). \quad \text{(A4)}$$

This is readily shown to be equal to

$$\Delta E_{slab}(x_s; x_b) = 2\Gamma(x_s; x_b) - \frac{x_0 - x_s}{x_0} 2\Gamma(0; x_b) - \frac{x_s}{x_0} 2\Gamma(x_0; x_b). \quad \text{(A5)}$$

It should be noted that no bulk term appears on the left-hand side in contrast to Eq. (A3) corresponding to homogeneous alloys.

Finally, we compare the formation energies of homogeneous and inhomogeneous slabs for the case when their surface concentrations are identical (on both surfaces of the slab), but concentration differences may occur in the interior. Differences arise primarily due to interfacial effects at the interface formed between the surface alloy and the bulk subsystem. First we introduce the energy per surface layer defined as [cf. Eq. (1)]

$$\bar{E}(x_s) \equiv \tfrac{1}{2}(E_{slab}(x_s) - (n_m - 2)E_b(x_s)) = E_b(x_s) + \Gamma(x_s), \quad \text{(A6)}$$

and rewrite the slab energies,

$$E_{slab}(x_s; x_b) = 2\bar{E}(x_s) + (n_m - 2)E_b(x_b) + 2\sigma(x_s; x_b). \quad \text{(A7)}$$

$\sigma(x_s; x_b)$ is referred to as an interfacial energy and defined by the previous equation. For equal indices, $\sigma(x; x) = 0$. The formation energies difference between homogeneous [Eq. (A2)] and inhomogeneous slabs [Eq. (A4)] using Eq. (A7) may then

be written as

$$\Delta E_{\mathrm{slab}}(x_{\mathrm{s}}) - \Delta E_{\mathrm{slab}}(x_{\mathrm{s}};x_{\mathrm{b}}) = (n_m - 2)\Delta E_{\mathrm{b}}(x_{\mathrm{s}}) - 2\Delta\sigma(x_{\mathrm{s}};x_{\mathrm{b}}) \tag{A8}$$

with

$$\Delta\sigma(x_{\mathrm{s}};x_{\mathrm{b}}) = \sigma(x_{\mathrm{s}};x_{\mathrm{b}}) - \frac{x_0 - x_{\mathrm{s}}}{x_0}\sigma(0;x_{\mathrm{s}}) - \frac{x_{\mathrm{s}}}{x_0}\sigma(x_0;x_{\mathrm{s}}). \tag{A9}$$

[1] S. K. Burke, R. Cywinski, J. R. Davis, and B. D. Rainford, The evolution of magnetic order in crfe alloys. ii. onset of ferromagnetism, J. Phys. F **13**, 451 (1983).

[2] C. Leygraf, G. Hultquist, S. Ekelund, and J. Eriksson, Surface composition studies of the (100) and (110) faces of monocrystalline $Fe_{0.84}Cr_{0.16}$, Surf. Sci. **46**, 157 (1974).

[3] S. Suzuki, T. Kosaka, H. Inoue, M. Isshiki, and Y. Waseda, Effect of the surface segregation of chromium on oxidation of high-purity Fe Cr alloys at room temperature, Appl. Surf. Sci. **103**, 495 (1996).

[4] R. Idczak, K. Idczak, and R. Konieczny, Oxidation and surface segregation of chromium in Fe-Cr alloys studied by Mössbauer and X-ray photoelectron spectroscopy, J. Nucl. Mater. **452**, 141 (2014).

[5] G. Wranglén, *An Introduction to Corrosion and Protection of Metals* (Chapman and Hall, London, 1985).

[6] R. J. Kurtz, A. Alamo, E. Lucon, Q. Huang, S. Jitsukawa, A. Kimura, R. Klueh, G. R. Odette, C. Petersen, M. A. Sokolov *et al.*, Recent progress toward development of reduced activation ferritic/martensitic steels for fusion structural applications, J. Nucl. Mater. **386**, 411 (2009).

[7] C. Leygraf, G. Hultquist, and S. Ekelund, A LEED/AES study of the oxidation of $fe_{0.84}cr_{0.16}$(100) and (110), Surf. Sci. **51**, 409 (1975).

[8] P. Dowben, M. Grunze, and D. Wright, Surface segregation of chromium in a Fe72Cr28 (110) crystal, Surf. Sci. **134**, L524 (1983).

[9] C. Xu and D. O'Connor, Surface structure and segregation of $Fe_{0.72}Cr_{0.28}$ (110), Nucl. Instrum. Methods Phys. Res., Sect. B **53**, 326 (1991).

[10] A. Davies, J. A. Stroscio, D. T. Pierce, and R. J. Celotta, Atomic-Scale Observations of Alloying at the Cr-Fe(001) Interface, Phys. Rev. Lett. **76**, 4175 (1996).

[11] D. Venus and B. Heinrich, Interfacial mixing of ultrathin Cr films grown on an Fe whisker, Phys. Rev. B **53**, R1733 (1996).

[12] B. Nonas, K. Wildberger, R. Zeller, and P. H. Dederichs, Energetics of 3 d Impurities on the (001) Surface of Iron, Phys. Rev. Lett. **80**, 4574 (1998).

[13] A. V. Ruban, H. L. Skriver, and J. K. Nørskov, Surface segregation energies in transition-metal alloys, Phys. Rev. B **59**, 15990 (1999).

[14] A. V. Ponomareva, E. I. Isaev, N. V. Skorodumova, Y. K. Vekilov, and I. A. Abrikosov, Surface segregation energy in bcc Fe-rich Fe-Cr alloys, Phys. Rev. B **75**, 245406 (2007).

[15] A. Kiejna and E. Wachowicz, Segregation of Cr impurities at bcc iron surfaces: First-principles calculations, Phys. Rev. B **78**, 113403 (2008).

[16] M. Levesque, M. Gupta, and R. P. Gupta, Electronic origin of the anomalous segregation behavior of Cr in Fe-rich Fe-Cr alloys, Phys. Rev. B **85**, 064111 (2012).

[17] W. R. Tyson, R. A. Ayres, and D. F. Stein, Anisotropy of cleavage in b.c.c. transition metals, Acta Metall. **21**, 621 (1973).

[18] M. Ropo, K. Kokko, M. P. J. Punkkinen, S. Hogmark, J. Kollár, B. Johansson, and L. Vitos, Theoretical evidence of the compositional threshold behavior of FeCr surfaces, Phys. Rev. B **76**, 220401 (2007).

[19] M. Ropo, K. Kokko, E. Airiskallio, M. P. Punkkinen, S. Hogmark, J. Kollár, B. Johansson, and L. Vitos, First-principles atomistic study of surfaces of fe-rich Fe-Cr, J. Phys.: Condens. Matter **23**, 265004 (2011).

[20] G. J. Ackland, Ordered sigma-type phase in the Ising model of Fe-Cr stainless steel, Phys. Rev. B **79**, 094202 (2009).

[21] G. J. Ackland, Magnetically Induced Immiscibility in the Ising model of FeCr Stainless Steel, Phys. Rev. Lett. **97**, 015502 (2006).

[22] P. Olsson, I. A. Abrikosov, and J. Wallenius, Electronic origin of the anomalous stability of Fe-rich bcc Fe-Cr alloys, Phys. Rev. B **73**, 104416 (2006).

[23] P. Müller and A. Saúl, Elastic effects on surface physics, Surf. Sci. Rep. **54**, 157 (2004).

[24] V. Fiorentini and M. Methfessel, Extracting convergent surface energies from slab calculations, J. Phys.: Condens. Matter **8**, 6525 (1996).

[25] M. Ropo, K. Kokko, L. Vitos, J. Kollár, and B. Johansson, The chemical potential in surface segregation calculations: AgPd alloys, Surf. Sci. **600**, 904 (2006).

[26] L. V. Pourovskii, A. V. Ruban, B. Johansson, and I. A. Abrikosov, Antisite-Defect-Induced Surface Segregation in Ordered NiPt Alloy, Phys. Rev. Lett. **90**, 026105 (2003).

[27] S. Schönecker, S. K. Kwon, B. Johansson, and L. Vitos, Surface parameters of ferritic iron-rich Fe-Cr alloy, J. Phys.: Condens. Matter **25**, 305002 (2013).

[28] L. D. Landau and E. M. Lifshitz, *Theory of Elasticity*, 3rd ed., Course of Theoretical Physics Vol. 7 (Pergamon Press, Oxford, 1986).

[29] A. Fasolino, A. Selloni, and A. Shkrebtii, 2.2 Surface reconstruction and relaxation, in *Landolt-Börnstein-Group III Condensed Matter: Numerical Data and Functional Relationships in Science and Technology*, Vol. 24a, edited by G. Chiarotti (Springer-Verlag, Berlin, 1993).

[30] R. Hafner, D. Spišak, R. Lorenz, and J. Hafner, Magnetic ground state of Cr in density-functional theory, Phys. Rev. B **65**, 184432 (2002).

[31] L. Vitos, H. L. Skriver, B. Johansson, and J. Kollár, Application of the exact muffin-tin orbitals theory: the spherical cell approximation, Comput. Mater. Sci. **18**, 24 (2000).

[32] L. Vitos, Total-energy method based on the exact muffin-tin orbitals theory, Phys. Rev. B **64**, 014107 (2001).

[33] L. Vitos, *Computational Quantum Mechanics for Materials Engineers: The EMTO Method and Applications* (Springer Science & Business Media, 2007).

[34] J. P. Perdew and Y. Wang, Accurate and simple analytic representation of the electron-gas correlation energy, Phys. Rev. B **45**, 13244 (1992).

[35] J. P. Perdew, K. Burke, and M. Ernzerhof, Generalized Gradient Approximation Made Simple, Phys. Rev. Lett. **77**, 3865 (1996).

[36] L. Vitos, J. Kollár, and H. L. Skriver, Full charge-density calculation of the surface energy of metals, Phys. Rev. B **49**, 16694 (1994).

[37] L. Vitos, J. Kollár, and H. L. Skriver, *Ab initio* full charge-density study of the atomic volume of α-phase Fr, Ra, Ac, Th, Pa, U, Np, and Pu, Phys. Rev. B **55**, 4947 (1997).

[38] P. Soven, Coherent-potential model of substitutional disordered alloys, Phys. Rev. **156**, 809 (1967).

[39] B. Gyorffy, Coherent-potential approximation for a nonoverlapping-muffin-tin-potential model of random substitutional alloys, Phys. Rev. B **5**, 2382 (1972).

[40] I. Mirebeau and G. Parette, Neutron study of the short range order inversion in $fe_{1-x}cr_x$, Phys. Rev. B **82**, 104203 (2010).

[41] S. M. Dubiel and J. Cieslak, Short-range order in iron-rich Fe-Cr alloys as revealed by Mössbauer spectroscopy, Phys. Rev. B **83**, 180202(R) (2011).

[42] G. Wang, S. Schönecker, S. Hertzman, Q.-M. Hu, B. Johansson, S. K. Kwon, and L. Vitos, *Ab initio* prediction of the mechanical properties of alloys: The case of Ni/Mn-doped ferromagnetic Fe, Phys. Rev. B **91**, 224203 (2015).

[43] X. Li, S. Schönecker, R. Li, X. Li, Y. Wang, J. Zhao, B. Johansson, and L. Vitos, *Ab initio* calculations of mechanical properties of bcc W–Re–Os random alloys: effects of transmutation of W, J. Phys.: Condens. Matter **28**, 295501 (2016).

[44] X. Li, S. Schönecker, J. Zhao, B. Johansson, and L. Vitos, Alloying effect on the ideal tensile strength of ferromagnetic and paramagnetic bcc iron, J. Alloys Compd. **676**, 565 (2016).

[45] P. Olsson, I. A. Abrikosov, L. Vitos, and J. Wallenius, *Ab initio* formation energies of Fe–Cr alloys, J. Nucl. Mater. **321**, 84 (2003).

[46] H. Zhang, B. Johansson, and L. Vitos, *Ab initio* calculations of elastic properties of bcc Fe-Mg and Fe-Cr random alloys, Phys. Rev. B **79**, 224201 (2009).

[47] M. P. Punkkinen, Q.-M. Hu, S. K. Kwon, B. Johansson, J. Kollár, and L. Vitos, Surface properties of 3 d transition metals, Philos. Mag. **91**, 3627 (2011).

[48] P. Błoński and A. Kiejna, Structural, electronic, and magnetic properties of bcc iron surfaces, Surf. Sci. **601**, 123 (2007).

[49] W. Tyson and W. Miller, Surface free energies of solid metals: Estimation from liquid surface tension measurements, Surf. Sci. **62**, 267 (1977).

[50] F. R. de Boer, R. Boom, W. C. M. Mattens, A. R. Miedema, and A. K. Niessen, *Cohesion in Metals: Transition Metal Alloys* (North-Holland, Amsterdam, 1988).

[51] O. Kovalenko, F. Chikli, and E. Rabkin, The equilibrium crystal shape of iron, Scr. Mater. **123**, 109 (2016).

[52] S. Schönecker, X. Li, B. Johansson, S. Kwon, and L. Vitos, Thermal surface free energy and stress of iron, Sci. Rep. **5**, 14860 (2015).

[53] Z. Q. Wang, S. H. Lu, Y. S. Li, F. Jona, and P. M. Marcus, Epitaxial growth of a metastable modification of copper with body-centered-cubic structure, Phys. Rev. B **35**, 9322 (1987).

[54] M. P. J. Punkkinen, S. K. Kwon, J. Kollár, B. Johansson, and L. Vitos, Compressive Surface Stress in Magnetic Transition Metals, Phys. Rev. Lett. **106**, 057202 (2011).

[55] J.-Y. Lee, M. P. J. Punkkinen, S. Schönecker, Z. Nabi, K. Kádas, V. Zólyomi, Y. M. Koo, Q.-M. Hu, R. Ahuja, B. Johansson, J. Kollár, L. Vitos, and S. K. Kwon, The surface energy and stress of metals, Surf. Sci. **674**, 51 (2018).

[56] A. Kuronen, S. Granroth, M. H. Heinonen, R. E. Perälä, T. Kilpi, P. Laukkanen, J. Lång, J. Dahl, M. P. J. Punkkinen, K. Kokko, M. Ropo, B. Johansson, and L. Vitos, Segregation, precipitation, and $\alpha - \alpha'$ phase separation in Fe-Cr alloys, Phys. Rev. B **92**, 214113 (2015).

[57] A. Christensen, A. V. Ruban, P. Stoltze, K. W. Jacobsen, H. L. Skriver, J. K. Nørskov, and F. Besenbacher, Phase diagrams for surface alloys, Phys. Rev. B **56**, 5822 (1997).

[58] C. Turtur and G. Bayreuther, Magnetic Moments in Ultrathin Cr Films on Fe(100), Phys. Rev. Lett. **72**, 1557 (1994).

[59] U. K. Poulsen, J. Kollár, and O. K. Andersen, Magnetic and cohesive properties from canonical bands, J. Phys.: Metal Phys. **6**, L241 (1976).

[60] O. K. Andersen, J. Madsen, U. K. Poulsen, O. Jepsen, and J. Kollár, Magnetic ground state properties of transition metals, Physica B **86-88**, 249 (1977).

[61] W. G. Wolfer, Elastic properties of surfaces on nanoparticles, Acta Mater. **59**, 7736 (2011).

[62] J. Staunton, B. L. Győrffy, A. J. Pindor, G. M. Stocks, and H. Winter, The "disordered local moment" picture of itinerant magnetism at finite temperatures, J. Magn. Magn. Mater. **45**, 15 (1984).

[63] B. L. Győrffy, A. J. Pindor, J. Staunton, G. M. Stocks, and H. Winter, A first-principles theory of ferromagnetic phase transitions in metals, J. Phys. F **15**, 1337 (1985).

[64] R. Soulairol, C.-C. Fu, and C. Barreteau, Magnetic and energetic properties of low-index Cr surfaces and Fe/Cr interfaces: A first-principles study, Phys. Rev. B **84**, 155402 (2011).

[65] Let $\Delta\epsilon$ be the energy separation of the d band centers associated with each type of atom and let w be their d bandwidth. In the 'common-band' model $\Delta\epsilon/w \ll 1$, whereas for 'split-band' behavior $\Delta\epsilon/w \gg 1$. An actual alloy electronic band structure is a complicated mixture of both models. For further reading, see for instance J. B. Staunton, S. S. A. Razee, M. F. Ling, D. D. Johnson, and F. J. Pinski, Magnetic alloys, their electronic structure and micromagnetic and microstructural models, J. Phys. D: Appl. Phys. **31**, 2355 (1998); D. G. Pettifor, *Bonding and Structure of Molecules and Solids* (Oxford University Press, Oxford, 1995).

[66] P. H. Dederichs, R. Zeller, H. Akai, and H. Ebert, Ab-initio calculations of the electronic structure of impurities and alloys of ferromagnetic transition metals, J. Magn. Magn. Mater. **100**, 241 (1991).

[67] X. Li, S. Schönecker, J. Zhao, B. Johansson, and L. Vitos, Anomalous ideal tensile strength of ferromagnetic Fe and Fe-rich alloys, Phys. Rev. B **90**, 024201 (2014).